nature physics

LETTERS

https://doi.org/10.1038/s41567-019-0605-6

Non-exponential decay of a giant artificial atom

Gustav Andersson[1*], Baladitya Suri[1,2], Lingzhen Guo[3*], Thomas Aref[1] and Per Delsing[1*]

In quantum optics, light–matter interaction has conventionally been studied using small atoms interacting with electromagnetic fields with wavelength several orders of magnitude larger than the atomic dimensions[1,2]. In contrast, here we experimentally demonstrate the vastly different 'giant atom' regime, where an artificial atom interacts with acoustic fields with wavelength several orders of magnitude smaller than the atomic dimensions. This is achieved by coupling a superconducting qubit[3] to surface acoustic waves at two points with separation on the order of 100 wavelengths. This approach is comparable to controlling the radiation of an atom by attaching it to an antenna. The slow velocity of sound leads to a significant internal time-delay for the field to propagate across the giant atom, giving rise to non-Markovian dynamics[4]. We demonstrate the non-Markovian character of the giant atom in the frequency spectrum as well as non-exponential relaxation in the time domain.

Cavity quantum electrodynamics (cavity QED) studies the interaction between atoms and photons in configurations where the atom is placed inside a cavity to enhance the interaction strength with the radiation field[5,6]. In parallel, artificial atoms based on superconducting circuits have emerged in the last 20 years and over the past 15 years superconducting circuit quantum electrodynamics has developed as an analogue to the cavity QED experiments[7]. This has enabled probing the strong and ultra-strong coupling regimes of atom–light interaction to study exotic phenomena including vacuum Rabi splitting[8] and the controlled generation of non-classical photon states[9,10]. A later development was waveguide QED where superconducting circuits were coupled to open transmission lines[11–13]. These experiments replace natural atoms and optical cavities with Josephson junction-based superconducting circuits behaving as artificial atoms strongly coupled to the field in open transmission lines or planar or three-dimensional microwave resonators[13,14].

For atoms coupled to laser light in optical cavity QED and the interaction of microwaves with either Rydberg atoms in cavities or artificial atoms in circuit QED, treating the atom as a point-like dipole is a valid approximation. In fact, in all the experiments mentioned above, the size of the atom L is at least an order of magnitude smaller than the wavelength λ of the interacting radiation.

More recently, a superconducting transmon qubit[15] was coupled to propagating surface acoustic waves (SAWs) on a piezoelectric substrate[16], demonstrating qubit decay by SAW emission and nonlinear reflection of SAW beams. Analogues of resonator QED architectures were realized in later experiments[17–21] where an artificial atom was coupled to the phonons inside an acoustic cavity[22]. Further work exploited superconducting qubits to generate and characterize phononic Fock states in SAW cavities as well as in bulk acoustic cavities[18,23]. Owing to the slow propagation speed of sound in solids (3,000 m s^{-1}), for a given frequency the wavelength of sound is five orders of magnitude smaller than that of light in vacuum. This property allows artificial atoms to interact with propagating acoustic fields beyond the small-atom approximation such that $L > \lambda$ (ref. [24]). Crucially to the experimental results presented here, the slow velocity of SAWs further enables the engineering of time delays that are significant compared with the relaxation time as laid out in ref. [4] proposing the giant atom configuration we have implemented here. In this case, the emitted excitation can be reabsorbed by the atom leading to non-Markovian effects.

Growing interest in quantum information science has spurred substantial theoretical investigations of non-Markovian open quantum systems, characterized by information back-flow from the environment[25]. In this context, the physical origin of the non-Markovianity is typically the coupling to a structured or finite reservoir. In contrast, we have realized a non-Markovian system by introducing deterministic time-delayed feedback through coupling a single quantum emitter at two distant points to a radiation field in one dimension. This feedback is intrinsic to the giant atom itself and can be engineered. In addition to enabling new parameter regimes in atom–field interactions, time-delayed feedback has potential applications in quantum information processing[26,27]. It has been suggested that this form of non-Markovianity could be exploited to generate cluster states for universal measurement-based quantum computation requiring considerably less hardware resources than gate-based approaches[27]. Recent work[28] has also demonstrated that architectures involving multiple giant atoms can be designed to realize interatomic interactions while protecting the atoms from decohering into the waveguide, provided their coupling points overlap in a braided configuration. This makes giant atoms a relevant candidate for applications in quantum simulations.

The artificial atom in this experiment is a transmon qubit, consisting of a superconducting quantum interference device (SQUID) loop connected in parallel with an interdigital transducer (IDT)[16,29]. This interdigitated finger structure provides a shunt capacitance for the transmon as well as coupling to SAWs at wavelengths matching the periodicity of the IDT, 1.25 µm. Owing to the fixed periodicity of the finger structure, the coupling is frequency-dependent and given by (see Supplementary Information)

$$\gamma(\omega) = \frac{N_p K^2 \omega_{01}}{4} \left(\frac{\sin X}{X}\right)^2 \quad (1)$$

where $\omega_{01}/2\pi$ is the qubit resonance frequency and $X = N_p\pi(\omega_{IDT} - \omega)/\omega_{IDT}$. This gives rise to a coupling strength that is proportional to the number of finger pairs N_p, with a coupling bandwidth that scales inversely with N_p. Our devices are fabricated using aluminium on GaAs that has a SAW velocity of $v_{SAW} = 2{,}900\,\mathrm{m\,s^{-1}}$. The piezoelectric coupling coefficient ($K^2 = 0.07\%$) of GaAs, while relatively low compared with materials such as lithium niobate and

[1]Department of Microtechnology and Nanoscience MC2, Chalmers University of Technology, Gothenburg, Sweden. [2]Department of Instrumentation and Applied Physics, Indian Institute of Science, Bengaluru, India. [3]Max Planck Institute for the Science of Light, Erlangen, Germany. *e-mail: gustav.andersson@chalmers.se; lingzhen.guo@mpl.mpg.de; per.delsing@chalmers.se

Table 1 | Giant atom sample parameters

Sample	N_p	$\gamma/2\pi$ (MHz)	T (ns)	γT	L (μm)	$\gamma_{gate}/2\pi$ (MHz)	$2\gamma/\gamma_{ext}$
A1	14	6.1	19	0.8	55	1.25	4.4
A2	14	4.4	46	1.4	125	1.5	1.8
A3	18	5.8	190	7.0	550	2.2	1.9
A4	18	5.3	190	6.3	550	-	-
B1	14	4.8	160	4.8	450	-	1.4

IDT finger pairs per coupling point N_p, acoustic coupling strength per coupling point γ, time delay T and coupling point separation L for the giant atom samples. All samples have an IDT centre frequency of 2.3 GHz. The resonator in sample B1 has a resonance frequency of 2.77 GHz. The coupling strength to the electrical gate γ_{gate} is shown for samples A1, A2, A3 in the second column from the right. The rightmost column shows the ratio of the total SAW coupling 2γ to the sum of non-acoustic decay rates $\gamma_{ext}=\gamma_{res}+\gamma_{gate}$. The parameters for samples A1, A2, A3 are extracted from fits to the gate reflection measurements shown in Fig. 2b, where γ is estimated by a fit of the resonance frequency to equation (3). The gate coupling γ_{gate} is estimated from the linewidth. The parameters for sample B1, which is coupled to a microwave resonator (with coupling strength $g=18$ MHz) rather than an electrical gate, are determined by two-tone spectroscopy of the absorption (Fig. 3a).

quartz[29], is still strong enough to ensure that the qubit lifetime τ is dominated by the acoustic coupling.

The giant atom is realized by splitting the IDT into two electrically connected coupling points separated by a distance L. Relevant sample parameters are listed in Table 1. Owing to the strong electromechanical coupling and slow propagation velocity of SAWs, the propagation time $T=L/v_{SAW}$ can be orders of magnitude larger than the excited-state lifetime. In such a case, a phonon emitted into the transmission line at one coupling point of the qubit due to the spontaneous decay may later be reabsorbed by the qubit at the second point. Considering the local IDT as a point-like coupling centre with coupling strength γ, the time-delay dynamics of the excited-state amplitude a_e in the absence of external driving is given by[4]

$$\frac{\partial a_e(t)}{\partial t} = -i\omega_{01}a_e(t) - \gamma(a_e(t) + a_e(t-T)) \qquad (2)$$

In the giant atom regime, characterized by $\gamma T \gtrsim 1$, the time-delayed coupling term in equation (2) introduces markedly non-Markovian effects, which is the subject of this paper.

The SAW–giant atom interaction is characterized using two different device designs. In design A, shown in Fig. 1a, the transmon is embedded in a SAW transmission line with IDTs to generate and pick up acoustic signals. In addition to IDTs on either side, a capacitively coupled gate provides electrical control. Using this design we first measure the SAW scattering properties to verify acoustic coupling. The steady-state emission properties are then characterized for a range of giant atom parameters by measurements via the electrical gate. For a chosen set of giant atom parameters, we implement a second device, design B (Fig. 1b), where the transmon is capacitively coupled to a coplanar waveguide $\lambda/4$ resonator. This enables us to read-out the state of the transmon by probing the resonator, which we exploit to perform spectroscopy on the giant atom as well as time-domain relaxation measurements. All the measured results are obtained at the 10 mK base temperature of a dilution refrigerator. The qubit resonance frequency is tuned into the SAW coupling band ($\omega_{01}/2\pi \approx 2.3$ GHz) using an applied external magnetic flux.

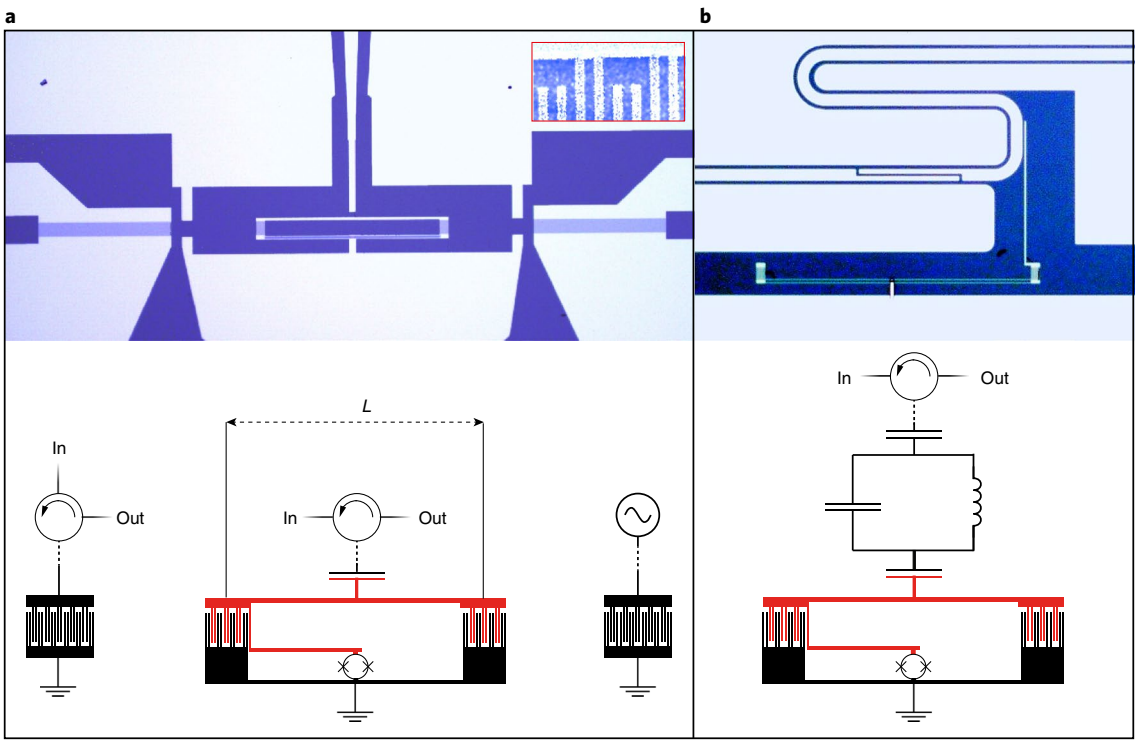

Fig. 1 | Device layouts. a, False-color optical micrograph (top) and circuit schematic (bottom) of a giant atom capacitively coupled to an electrical gate. The GaAs substrate is shown in blue and the aluminium circuit and ground planes are white. The transmon circuit that makes up the giant atom with coupling point separation L is grounded and has two Josephson junctions forming a SQUID loop to enable frequency tuning via an external coil. The acoustic reflection and transmission properties are probed via IDTs on either side of the giant atom. A circulator routes the reflected gate signal to a cryogenic amplifier. The inset (top) shows a false-colour scanning electron micrograph of the finger structure of the giant atom IDTs. **b**, False-colour optical micrograph (top) and circuit schematic (bottom) of a giant atom coupled to a coplanar waveguide resonator. Excitation and read-out tones are sent via a circulator to the resonator input. The reflected read-out signal is amplified and measured similarly to the gate reflection in **a**.

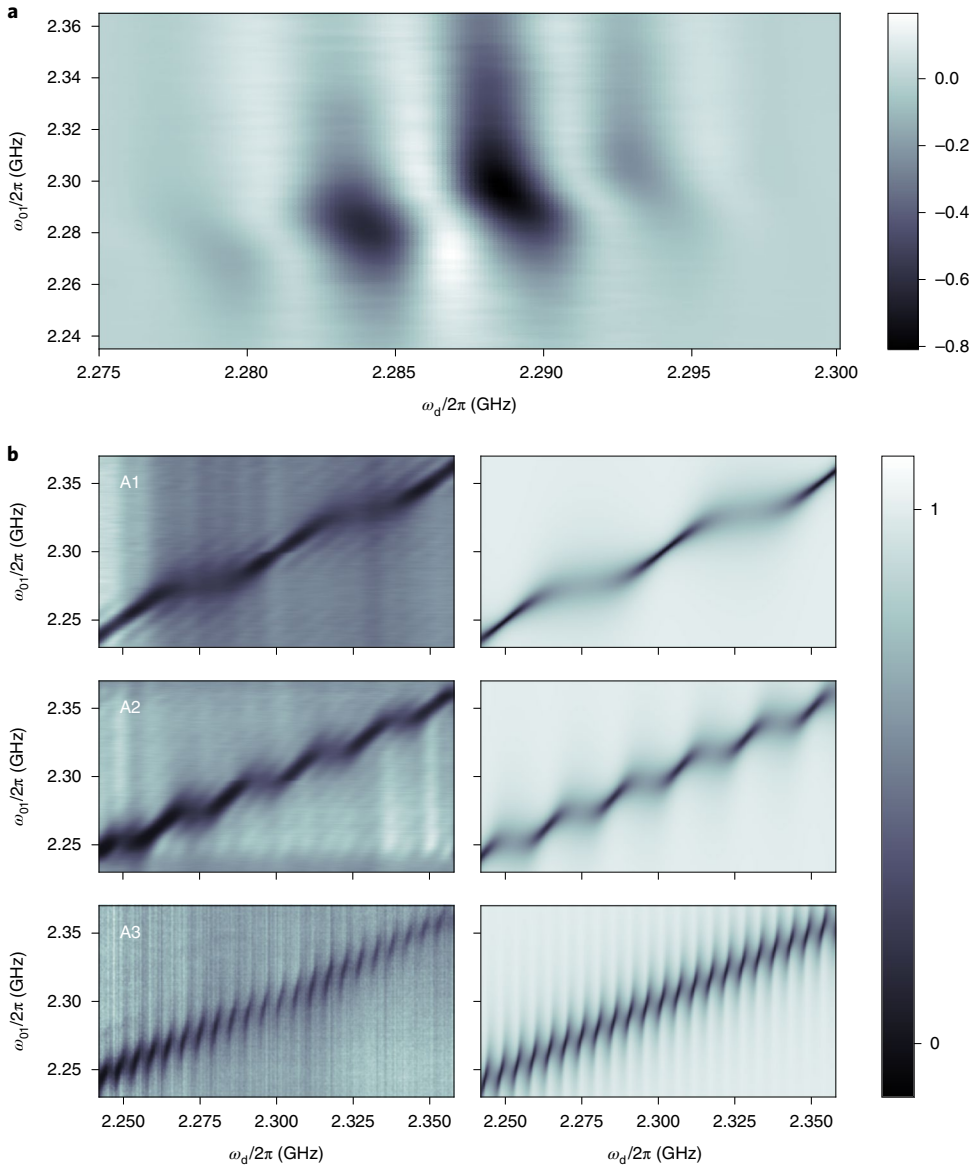

Fig. 2 | Scattering properties of the giant atom. a, Acoustic power transmission (normalized) of a SAW signal from the launcher IDT to the pick-up IDT measured as a function of SAW frequency $\omega_d/2\pi$ and giant atom frequency $\omega_{01}/2\pi$ for sample A4. The background transmission when the giant atom is far detuned from the SAW frequency range has been subtracted. The small positive values for certain frequencies is an artefact of this subtraction (see Supplementary Information). The magnitude is normalized to the maximal SAW transmission of the subtracted, far-detuned trace. The two visible dips in transmission are separated by $1/T \approx 5$ MHz. The limited bandwidth of the launcher and pick-up IDTs allows the acoustic scattering to be mapped across a frequency span of approximately 14 MHz. **b**, Reflected electromagnetic power (normalized) off the capacitively coupled electrical gate for three different giant atoms (A1–A3). The reflectance is measured while sweeping the drive frequency ω_d and giant atom frequency ω_{01} (left). Theoretical reflectance given by equation (16) found in the Supplementary Information is shown in the right panels. Sample parameters are listed in Table 1. The residual dissipation included to generate the theory plots are $\gamma_d/2\pi = \{1.5\,\text{MHz}, 3.5\,\text{MHz}, 4.0\,\text{MHz}\}$ for A1, A2, A3. Increasing the coupling point separation, and thereby the time delay T, gives rise to a finer structure in the interference pattern. The background reflection when the giant atom is far detuned from the SAW frequency range has been subtracted.

The steady-state acoustic transmission amplitude is measured at the pick-up IDT while a continuous weak SAW drive is applied to the giant atom using the launcher IDT. In Fig. 2a we map the acoustic transmission amplitude for sample A4 as a function of drive frequency $\omega_d/2\pi$ while tuning the qubit resonance frequency $\omega_{01}/2\pi$. At weak driving powers, we expect to approach the limit of near-perfect extinction of transmitted SAWs when ω_d matches ω_{01} (refs. [11,30]). However, for our giant atom, we observe that interference between the scattering of each point causes the condition for total reflection of a coherent beam to be modified from $\omega_d = \omega_{01}$. A right-propagating SAW beam of frequency $\omega/2\pi$ transmitted at $x = 0$ (left coupling point) will pick up a phase factor $e^{i\omega T}$ before interacting with the giant atom again at $x = L$. The phase factors add up to yield a maximum reflection condition of[4]

$$\omega_{01} = \omega_d - \gamma \sin \omega_d T \tag{3}$$

The coupling point separation of sample A4 ($L = 550\,\mu\text{m}$) is sufficiently large that interference fringes are visible within the bandwidth constrained by the launcher and pick-up IDTs.

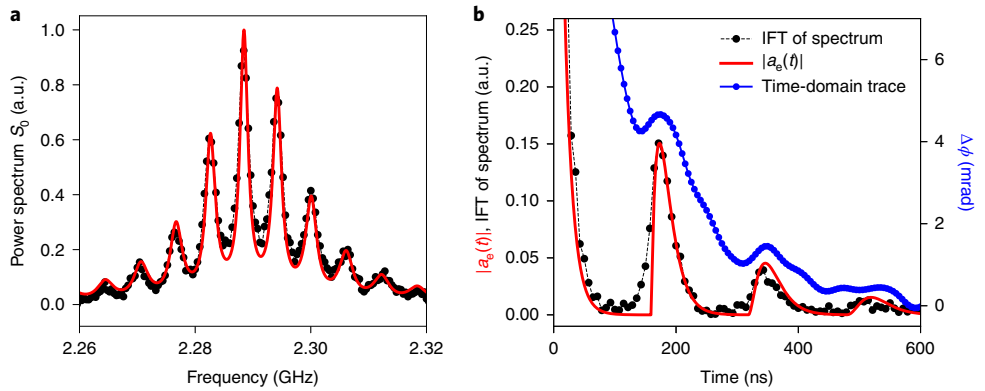

Fig. 3 | Frequency response and dynamics of the giant atom. a, Two-tone spectroscopy of the giant atom measured through the electromagnetic resonator. A fixed-frequency read-out is applied on resonance with the resonator, while a probe tone is swept across the giant atom resonance $\omega_{01}/2\pi = 2.29$ GHz. The dotted black line shows the spectrum (normalized) of a giant atom with $L = 450$ μm (sample B1) obtained from the read-out phase response. A fit to equation (5) is shown as the red line. The multi-peak structure arises due to the interference of SAW emission from the giant atom coupling points. **b**, Time evolution of the giant atom excited-state population. The dotted black line shows the magnitude of the inverse Fourier transform (IFT) of the (complex-valued) spectrum plotted in **a**. The red line shows the time evolution of $|a_e(t)|$ corresponding to the spectrum S_0 in **a**. This implies the (magnitude square) Fourier transform of a_e gives the fit to S_0. The relaxation obtained in the time domain via the phase $\Delta\varphi$ of a read-out tone to the resonator is shown in blue. The elevated power in the read-out tone causes a slowdown in the qubit–resonator interaction, leading to the slowly decaying envelope in the response.

Next, we study the SAW emission from the giant atom. A continuous drive of frequency $\omega_d/2\pi$ is applied to the capacitively coupled electrical gate while measuring the reflected amplitude of the drive tone. Efficient conversion of the input signal to SAWs will result in a dip in the gate reflection, allowing for the characterization of the steady-state emission of the giant atom (Fig. 2b). Similarly to the acoustic reflection off a giant atom, this does not generally occur for $\omega_{01} = \omega_d$ (see Supplementary Information).

The condition for maximal transduction of the electrical signal to outgoing SAWs coincides with maximal acoustic reflection and is given by equation (3). In addition, the giant atom coupling to the SAW depends on the drive frequency as

$$\gamma_{\mathrm{eff}} = \gamma(1 + \cos\omega_d T) \tag{4}$$

As this measurement is not limited by the bandwidth of the launcher IDTs, the giant atom properties may be probed across a wider frequency range than in the purely acoustic case. We exploit this to measure gate reflection for three samples with intrinsic time delays of $T \approx \{19\,\mathrm{ns}, 45\,\mathrm{ns}, 190\,\mathrm{ns}\}$. Going deeper into the giant atom regime, that is, increasing T, leads to a finer interference structure in the gate reflection, which is shown in Fig. 2b. Fitting the resonance frequency modulation to data from the largest atom, the designed separation distance (550 μm) yields a SAW velocity of 2,906 m s^{-1} on GaAs, consistent with literature values at millikelvin temperatures[29].

Coupling the giant atom to an electromagnetic resonator in addition to the SAW field enables spectroscopy in the dispersive regime of circuit QED. This allows us to measure the excited-state population. In sample B1, a $\lambda/4$ resonator with resonance frequency $f_r = 2.77$ GHz is capacitively coupled to the giant atom with coupling strength $g/2\pi = 15$ MHz. Operating the giant atom at IDT resonance (2.29 GHz) gives an atom–cavity detuning of 480 MHz, resulting in a dispersive shift $\chi/2\pi = 0.47$ MHz. This is small compared with the SAW–atom interaction strength but sufficiently large to read-out the qubit state via the resonator phase response. The spectrum of sample B1 is probed in two-tone spectroscopy with a weak, fixed-frequency read-out tone applied at f_r while a drive tone is swept across the resonance of the giant atom. The interaction with phonons already emitted into the SAW channel gives rise to a multi-peak structure in the absorption very different from the Lorentzian lineshape of ordinary (small) atoms. In Fig. 3a the phase of the read-out tone is shown along with a fit to the expression

$$S_0(\omega) = \frac{\omega_{01}}{|\omega - \omega_{01} + i\gamma(1 + \mathrm{e}^{i\omega T}) + i\gamma_{\mathrm{res}}|^2} \tag{5}$$

where $\gamma_{\mathrm{res}} \approx 2\pi \times 6.85$ MHz represents residual broadening of the spectral lineshape induced by non-acoustic decay as well as the finite spectroscopic drive power.

The spectrum of the giant atom excitation is related to its time evolution via the Fourier transform, such that $S_0 = \left|\int_{-\infty}^{\infty} a_e(t)\mathrm{e}^{i\omega t}\mathrm{d}t\right|^2$. The excitation amplitude of an initially excited giant atom evolves according to

$$a_e(t) = \sum_{n=0}^{\infty} \Theta(t - nT)\frac{(-\gamma(t - nT))^n}{n!}\mathrm{e}^{-i(\omega_{01} - i\gamma - i\gamma_{\mathrm{res}})(t - nT)} \tag{6}$$

where $\Theta(t)$ is the Heaviside function. For times $t > T$, interference between the instantaneous relaxation and the amplitude already emitted into the acoustic field gives rise to sub-exponential decay. While the inital decay is exponential with a rate fixed by γ, each revival peak decays slower than exponentially and, on sufficiently short timescales, the peak amplitude is only polynomially damped. The time evolution of $|a_e(t)|$ that corresponds to the power spectrum of Fig. 3a is shown as the red line in Fig. 3b. It captures well the features of the inverse Fourier transform (IFT) of the measured giant atom power spectrum (black dotted line, Fig. 3b). In the Supplementary Information we show that the trace distance between the initially excited state and the ground state evolves non-monotonically in time, providing a quantitative measure of the non-Markovianity of the giant atom[31].

To directly probe the non-exponential decay in the time domain, we monitor continuously the phase response of the read-out resonator while applying an approximate π-pulse to the giant atom. The data are averaged approximately 10^7 times and shown as the blue line in Fig. 3b. The read-out tone is applied with high power[32] such that the qubit–cavity system enters the nonlinear regime where switching between metastable states occurs. In this regime the resonator acquires a memory of the qubit state longer than the qubit relaxation time, giving rise to a slowly decaying exponential envelope.

This appears as a smearing effect in the time trace. Two revivals of the giant atom are clearly visible in this measurement, occurring at times consistent with the spectroscopic data.

Our results show that the acousto–electric interaction can be exploited to investigate previously unexplored parameter regimes of light–matter interaction. We have demonstrated that superconducting qubits can be strongly coupled to SAWs such that the giant atom regime can be reached with significant internal time delays giving rise to non-Markovian dynamics. In the present experiment we have studied spontaneous emission from a single giant atom. Further new physics can be expected in circuit- and waveguide-QED settings for systems that break the Markov approximation. For example, it would be interesting to study waveguide-mediated interactions between quantum emitters in the non-Markovian regime, or the quantum properties of sound reflected from a giant atom.

Data availability

The data generated and analysed in this study are available from the corresponding authors upon reasonable request.

Online content

Any methods, additional references, Nature Research reporting summaries, source data, statements of code and data availability and associated accession codes are available at https://doi.org/10.1038/s41567-019-0605-6.

Received: 3 November 2018; Accepted: 26 June 2019;
Published online: 12 August 2019

References

1. Brune, M., Haroche, S., Lefevre, V., Raimond, J. M. & Zagury, N. Quantum nondemolition measurement of small photon numbers by Rydberg-atom phase-sensitive detection. *Phys. Rev. Lett.* **65**, 976–979 (1990).
2. Raimond, J. M., Brune, M. & Haroche, S. Manipulating quantum entanglement with atoms and photons in a cavity. *Rev. Mod. Phys.* **73**, 565–582 (2001).
3. Schoelkopf, R. J. & Girvin, S. M. Wiring up quantum systems. *Nature* **451**, 664–669 (2008).
4. Guo, L., Grimsmo, A. L., Kockum, A. F., Pletyukhov, M. & Johansson, G. Giant acoustic atom: a single quantum system with a deterministic time delay. *Phys. Rev. A* **95**, 053821 (2017).
5. Goy, P., Raimond, J. M., Gross, M. & Haroche, S. Observation of cavity-enhanced single-atom spontaneous emission. *Phys. Rev. Lett.* **50**, 1903–1906 (1983).
6. Miller, R. et al. Trapped atoms in cavity QED: coupling quantized light and matter. *J. Phys. B* **38**, S551 (2005).
7. Gu, X., Kockum, A., Miranowicz, A., Liu, Y. & Nori, F. Microwave photonics with superconducting quantum circuits. *Phys. Rep.* **718**, 1–102 (2017).
8. Wallraff, A. et al. Strong coupling of a single photon to a superconducting qubit using circuit quantum electrodynamics. *Nature* **431**, 162–167 (2004).
9. Hofheinz, M. et al. Synthesizing arbitrary quantum states in a superconducting resonator. *Nature* **459**, 546–549 (2009).
10. Wang, C. et al. A Schrödinger cat living in two boxes. *Science* **352**, 1087–1091 (2016).
11. Hoi, I. C. et al. Demonstration of a single-photon router in the microwave regime. *Phys. Rev. Lett.* **107**, 073601 (2011).
12. Abdumalikov, A. A. et al. Electromagnetically induced transparency on a single artificial atom. *Phys. Rev. Lett.* **104**, 193601 (2010).
13. Roy, D., Wilson, C. M. & Firstenberg, O. Colloquium: strongly interacting photons in one-dimensional continuum. *Rev. Mod. Phys.* **89**, 021001 (2017).
14. Paik, H. et al. Observation of high coherence in Josephson junction qubits measured in a three-dimensional circuit QED architecture. *Phys. Rev. Lett.* **107**, 240501 (2011).
15. Koch, J. et al. Charge-insensitive qubit design derived from the Cooper pair box. *Phys. Rev. A* **76**, 042319 (2007).
16. Gustafsson, M. V. et al. Propagating phonons coupled to an artificial atom. *Science* **346**, 207–211 (2014).
17. Manenti, R. et al. Circuit quantum acoustodynamics with surface acoustic waves. *Nat. Commun.* **8**, 975 (2017).
18. Chu, Y. et al. Quantum acoustics with superconducting qubits. *Science* **358**, 199–202 (2017).
19. Moores, B. A., Sletten, L. R., Viennot, J. J. & Lehnert, K. W. Cavity quantum acoustic device in the multimode strong coupling regime. *Phys. Rev. Lett.* **120**, 227701 (2018).
20. Bolgar, A. N. et al. Quantum regime of a two-dimensional phonon cavity. *Phys. Rev. Lett.* **120**, 223603 (2018).
21. Noguchi, A., Yamazaki, R., Tabuchi, Y. & Nakamura, Y. Qubit-assisted transduction for a detection of surface acoustic waves near the quantum limit. *Phys. Rev. Lett.* **119**, 180505 (2017).
22. Manenti, R. et al. Surface acoustic wave resonators in the quantum regime. *Phys. Rev. B* **93**, 041411 (2016).
23. Satzinger, K. J. et al. Quantum control of surface acoustic wave phonons. *Nature* **563**, 661–665 (2018).
24. Kockum, A. F., Delsing, P. & Johansson, G. Designing frequency-dependent relaxation rates and Lamb shifts for a giant artificial atom. *Phys. Rev. A* **90**, 013837 (2014).
25. Breuer, H.-P., Laine, E.-M., Piilo, J. & Vacchini, B. Colloquium: non-Markovian dynamics in open quantum systems. *Rev. Mod. Phys.* **88**, 021002 (2016).
26. Pichler, H. & Zoller, P. Photonic circuits with time delays and quantum feedback. *Phys. Rev. Lett.* **116**, 093601 (2016).
27. Pichler, H., Choi, S., Zoller, P. & Lukin, M. D. Universal photonic quantum computation via time-delayed feedback. *Proc. Natl Acad. Sci. USA* **114**, 11362–11367 (2017).
28. Kockum, A. F., Johansson, G. & Nori, F. Decoherence-free interaction between giant atoms in waveguide quantum electrodynamics. *Phys. Rev. Lett.* **120**, 140404 (2018).
29. Aref, T. et al. in *Superconducting Devices in Quantum Optics* (eds Hadfield, R. H. & Johansson, G.) 217–244 (Springer International Publishing, 2016).
30. Astafiev, O. et al. Resonance fluorescence of a single artificial atom. *Science* **327**, 840–843 (2010).
31. Breuer, H.-P., Laine, E.-M. & Piilo, J. Measure for the degree of non-Markovian behavior of quantum processes in open systems. *Phys. Rev. Lett.* **103**, 210401 (2009).
32. Reed, M. D. et al. High-fidelity readout in circuit quantum electrodynamics using the Jaynes-Cummings nonlinearity. *Phys. Rev. Lett.* **105**, 173601 (2010).

Acknowledgements

This work was supported by the Knut and Alice Wallenberg foundation and by the Swedish Research Council (VR). This project has also received funding from the European Union's Horizon 2020 research and innovation programme under grant agreement no. 642688. We acknowledge fruitful discussions with M. K. Ekström and G. Johansson.

Author contributions

G.A., B.S. and T.A. contributed to the design and fabrication of devices. L.G. developed the theoretical expressions for spectra and relaxation rates. G.A. and B.S. performed the measurements. All authors contributed to discussions and the interpretation of results. P.D. supervised the project, and G.A., B.S., L.G. and P.D. contributed to the writing of the manuscript.

Competing interests

The authors declare no competing interests.

Additional information

Supplementary information is available for this paper at https://doi.org/10.1038/s41567-019-0605-6.

Reprints and permissions information is available at www.nature.com/reprints.

Correspondence and requests for materials should be addressed to G.A., L.G. or P.D.

Peer review information: *Nature Physics* thanks Adam Miranowicz and the other, anonymous, reviewer(s) for their contribution to the peer review of this work.

Publisher's note: Springer Nature remains neutral with regard to jurisdictional claims in published maps and institutional affiliations.